Dynamics of exciton energy renormalization in monolayer transition metal disulfides

Jiaxin Zhao[1,§], Weijie Zhao[1,§], Wei Du[1], Rui Su[1], and Qihua Xiong[1,2] (✉)

[1] *Division of Physics and Applied Physics, School of Physical and Mathematical Sciences, Nanyang Technological University, Singapore 637371, Singapore*

[2] *State Key Laboratory of Low-Dimensional Quantum Physics and Department of Physics, Tsinghua University, Beijing 100084, China*

[§] *Jiaxin Zhao and Weijie Zhao contributed equally to this work.*

ABSTRACT

Fundamental understandings on the dynamics of charge carriers and excitonic quasiparticles in semiconductors are of central importance for both many-body physics and promising optoelectronic and photonic applications. Here, we investigated the carrier dynamics and many-body interactions in two-dimensional (2D) transition metal dichalcogenides (TMDs), using monolayer WS_2 as an example, by employing femtosecond broadband pump-probe spectroscopy. Three time regimes for the exciton energy renormalization are unambiguously revealed with a distinct red-blue-red shift upon above-bandgap optical excitations. We attribute the dominant physical process in the three typical regimes to free carrier screening effect, Coulombic exciton–exciton interactions and Auger photocarrier generation, respectively, which show distinct dependence on the optical excitation wavelength, pump fluences and/or lattice temperature. An intrinsic exciton radiative lifetime of about 1.2 picoseconds (ps) in monolayer WS_2 is unraveled at low temperature, and surprisingly the efficient Auger nonradiative decay of both bright and dark excitons puts the system in a nonequilibrium state at the nanosecond timescale. In addition, the dynamics of trions at low temperature is observed to be significantly different from that of excitons, e.g., a long radiative lifetime of ~ 108.7 ps at low excitation densities and the evolution of trion energy as a function of delay times. Our findings elucidate the dynamics of excitonic quasiparticles and the intricate many-body physics in 2D semiconductors, underpinning the future development of photonics, valleytronics and optoelectronics based on 2D semiconductors.

KEYWORDS

transitional metal disulfide, exciton dynamics, renormalization, transient absorption spectroscopy, carrier screening effect, exciton–exciton interactions

1 Introduction

Monolayer group VI transition metal dichalcogenides (TMDs) are emerging two-dimensional (2D) semiconductors with a sizable direct bandgap and exceptional physical properties [1–6]. Owing to the reduced dimensionality and significantly suppressed dielectric screening in monolayer TMDs, excitons, namely Coulomb-bound electron–hole pairs, show enormous binding energy of several hundred meV and strong light–matter interactions [6, 7]. Consequently, the optical and electronic properties are mostly dominated by excitons, rendering great opportunities for novel optoelectronic and photonic applications [1–3, 5–8]. Recently, tremendous research efforts have been made to developing high-performance photodetectors [9, 10], light-emitting diodes [11, 12], valleytronic transistors [6, 13–15], optical interconnects [16], excitonic lasers [17, 18], etc. On the other hand, the tightly bound exciton offers an ideal system to investigate many-body physics [7, 19–21]. For instance, multi-particle excitonic complexes, like charged exciton (trions), biexcitons and charged biexcitons, are observed and show distinct optical properties for potential device applications [22–26]. Fundamental understanding of carrier/exciton dynamics, many-body correlations and the resultant optical nonlinearities are critically important to facilitate the intelligent design and utilization of novel valleytronic, optoelectronic and photonic devices with desirable functionalities.

In the past few years, the carrier and exciton dynamics in monolayer TMDs are studied extensively by using ultrafast pump-probe spectroscopy which is an ideal tool to investigate the intrinsic ultrafast optical phenomena in the 2D regime. The ultrafast formation and recombination of excitons [27–31], many-body correlations between excitonic complexes [32–35], valley/spin depolarization dynamics [33, 36–39], giant bandgap renormalization and transient optical gain under intense optical excitations [20, 40], as well as ultrafast interface charge transfer in TMDs van der Waals heterostructures [41], are revealed responsible for the corresponding macroscopic optical properties and device performances. However, a comprehensive physical picture for the exciton dynamics and transient optical nonlinearities is still absent. First, the influence of carrier screening effects on the optical response of exciton resonance is reported inconsistently under different experimental conditions, such as the sample quality, excitation wavelength and temporal resolutions [40, 42, 43]. Secondly, the nature of exciton–exciton interactions, either Coulombic repulsion or atom-like attraction, is still controversial [43–46]. Thirdly, when the excitation

densities are in the intermediate and high regimes, the explicit assignment of Auger-type nonradiative mechanisms for excitons is required to fully understand the associated nonlinear optical phenomena [30, 47–51]. For instance, the photoexcited electron–hole system of monolayer TMDs remains in an unexpected nonequilibrium state at the nanosecond (ns) timescale [28, 30]. More importantly, the dynamics of other quasiparticles, such as trions, remains largely unexplored since most pump-probe experiments are done at room temperature [31, 33, 35, 40, 42, 43]. Detailed studies of trion dynamics as a function of lattice temperature and pump fluence could provide critical information for the many-body correlations and unprecedented valley physics in 2D TMDs.

In this report, we address these important questions by presenting a systematic study of the exciton and trion dynamics in monolayer WS_2 using broadband femtosecond transient absorption (TA) spectroscopy. The temporal evolution of the pump-induced changes of exciton and trion absorption is examined as a function of excitation wavelength, pump fluence and lattice temperature. We observe a distinct red-blue-red shift of the exciton resonance in different time regimes under non-resonant excitations. In the first sub-picosecond regime, the redshift and broadening of exciton resonance, which disappear under resonant excitations, are attributed to screening effects of hot carriers. Following the quick relaxation of free carriers and buildup of exciton population within the first picosecond (ps), the repulsive exciton–exciton interaction leads to a slight blueshift of exciton energy at low temperature. Interestingly, the effective lifetime of bright excitons in monolayer WS_2 becomes longer when the pump fluence increases, which persists to several tens of ps. In the third regime at longer delay times (> ~ 10.0 ps), a redshift of exciton energy develops and shows a super-linear dependence on pump fluence, suggesting that Auger recombination of excitons generates nonequilibrium free carriers, instead of heating the lattice. Furthermore, the trion dynamics, distinct from exciton dynamics, shows an increase of trion binding energy in the first sub-ps time regime and subsequently a much longer decay time of ~ 108.7 ps at low pump fluence and low temperature.

2 Results and discussions

The monolayer TMDs are prepared by mechanical exfoliations of commercially available bulk crystals and then transferred onto sapphire substrates. The exfoliated samples are characterized by using steady-state photoluminescence (PL) and absorption spectroscopy. Figure 1(a) shows the absorption spectra of monolayer WS_2 at room and low temperatures which are extracted from transmission spectra. More results about the optical micrograph and the photoluminescence spectrum of the monolayer WS_2 at room temperature are shown in the Fig. S1 in the Electronic Supplementary Material (ESM). At room temperature, the two absorption peaks at around 1.97 and 2.4 eV are known as A and B excitons, respectively, arising from the direct optical transitions at K points of the Brillouin zone as schematically shown in Fig. 1(b). Due to strong spin-orbit coupling in WS_2, the spin-splitting of valence and conduction bands leads to a large energy difference between bright A and B excitons, while the resulted spin-forbidden dark exciton has the lowest transition energy as indicated by the dashed arrows. These characteristics largely determine the unique optical properties of monolayer WS_2. At 10 K, the exciton energies show considerable blueshift following the increasing of the electronic bandgap (E_g) shown in Fig. 1(a). In addition, a new absorption peak appears slightly below A excitons and is attributed to the charged exciton states (trions). It has been well established

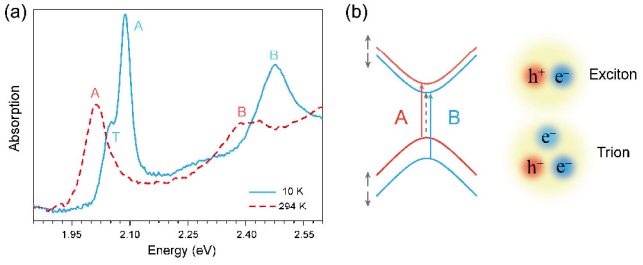

Figure 1 The steady-state absorption spectra of monolayer WS_2. (a) The absorption spectra of monolayer WS_2 on a sapphire substrate measured at 10 K (blue solid curve) and 294 K (red dashed curve). The A, B and T indicate the absorption peaks for A and B exciton and trion states. (b) Schematics of the electronic band structure at K points of the Brillouin zone (left) and exciton and negative trion states (right) for monolayer WS_2. The red and blue curved bands show the spin-splitting of the valence or conduction bands due to the spin-orbit interactions, and the corresponding spin orientation is indicated by the short grey arrows. The optical transitions associated with bright A and B excitons are marked by the red and blue arrows, respectively. The grey dashed arrow shows the spin-forbidden dark excitons which cannot be directly accessed by optical excitations. The dark excitons as the energetically lowest states play an important role in the exciton dynamics in monolayer WS_2.

that the exfoliated WS_2 and MoS_2 samples on various substrates present unintentional electron doping from sulfur vacancies or substrate and impurities induced doping [21, 22]. Therefore, the exciton can capture one additional electron through the Coulomb force to form a negative trion as schematically shown in Fig. 1(b). The trion binding energy (E_B) is ~ 42.8 meV in our sample, which is the energy difference between the exciton and trion absorption peaks. The intensity ratio between the exciton and trion absorption peaks, analyzed by the multi-Lorentzian fitting and shown in Fig. S2 in the ESM, allows us to estimate the electron doping concentration in the range of 5×10^{11}–8×10^{11} cm^{-2} [21], which is further supported by the TA measurements to be discussed in the following text.

We further investigated the exciton and trion dynamics in monolayer WS_2 by using broadband femtosecond TA spectroscopy as a function of lattice temperature, excitation energy and density. In our TA measurements, charge carriers and excitons are injected into monolayer TMDs by using a femtosecond pump beam with a pulse width of ~ 100.0 fs. The broadband probe beam (1.65–2.85 eV) is generated from an optically pumped sapphire crystal. The two beams are collinearly focused into the samples with cross-linear polarizations. The measured differential transmissions $\frac{\Delta T}{T} = \frac{T_{\text{pump-on}} - T_{\text{pump-off}}}{T_{\text{pump-off}}}$ at controlled delay times (Δt) present a combination of changes of exciton/trion populations, resonance energies and so forth, allowing us to monitor the evolution of optical nonlinearities in the excited system.

Figure 2(a) shows a contour plot of TA spectra of a monolayer WS_2 under the above-bandgap excitation of 3.35 eV at 10 K. The pump fluence is ~ 12.7 μJ/cm², corresponding to an estimated carrier density (n_p) of ~ 3.6×10^{12} cm^{-2}. Following the optical excitation, the pump-induced bleaching (PIB) and absorption (PIA) features, corresponding to positive and negative $\Delta T/T$, respectively, appears instantaneously around the A exciton (E_A = 2.09 eV) and trion (E_T = 2.05 eV) resonances. Three-time regimes can be identified according to the distinct PIB and PIA features as a function of delay time. (I) First of all, a sub-ps decay feature, especially a prominent PIA at energies below 2.03 eV, is observed; (II) secondly, in the time regime of ~ 1.0 ps to several tens of ps, the PIB peaks corresponding to the excitons and trions, as well as the PIA feature at energies larger than 2.10 eV, decay as a function of delay times; (III) thirdly, for

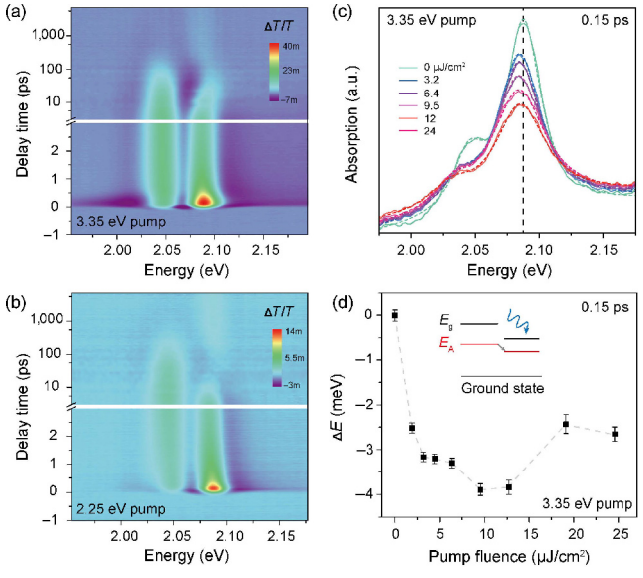

Figure 2 Carrier-screening induced redshift of the exciton resonance in the first sub-ps regime. (a) and (b) Time evolution of the TA spectra of monolayer WS_2 at 10 K. The photon energy of pump beams (E_{pump}) is 3.35 eV (a) and 2.25 eV (b), respectively, and the pump fluence is kept as ~ 12.7 μJ/cm^2. (c) Absorption spectra around the A exciton resonance energy of monolayer WS_2 at Δt = 0.15 ps as a function of pump fluence for E_{pump} = 3.35 eV. The experimental data (solid curves) are fitted with two Lorentzian peaks (dashed curves) for excitons and trions. The vertical dashed line is a guide to the eye. (d) The energy shifts (ΔE), which are the energy difference of the A exciton resonance with and without pump, as a function of pump fluence extracted from the fitting curves in (c). The inset in (d) shows the schematics of electronic band structure of monolayer WS_2 and the energy renormalization of the bandgap (E_g) and exciton resonance (E_A) at the presence of pump injected free carriers. The gray dashed curve is a guide to the eye.

the delay times longer than several tens of ps, a derivative feature centered at E_A rises over a few tens of ps and decays over hundreds of ps. Two more sets of TA spectra as a function of pump fluence (1.9 and 24.0 μJ/cm^2) are shown in Fig. S3 in the ESM, particularly one can clearly observe the typical three time regimes in a line cut along delay time axis. We also observed similar dynamics of A excitons for monolayer WS_2 and MoS_2 at room temperature shown in Figs. S4 and S5 in the ESM, respectively. The rich nonlinear optical phenomena observed here signify the complicated exciton dynamics and intriguing many-body physics in 2D TMDs.

We first discussed the underlying physics of the first sub-ps decay feature. By further performing the excitation-energy dependent TA measurements, the PIA feature at the low energy side gradually diminishes when the photon energy of pump excitations approaches the exciton resonance, while the dynamics observed in the second- and third-time regimes remains the same as shown in Fig. 2(b) and Fig. S6 in the ESM. Therefore, unambiguously this ultrafast decay can be correlated to optical nonlinear effects induced by the presence of non-equilibrium hot carriers in the system. Generally, the carrier screening effect in semiconductors not only leads to significant renormalization of the bandgap but also reduces the oscillator strength and binding energy (E_B) of excitons [45, 46]. However, the resulted overall change of the optical response could be drastically different in various semiconductors [42, 45, 46]. In Fig. 2(c), we extract the absorption spectra for Δt = 0.15 ps at which the $\Delta T/T$ of the sub-ps PIB feature rises to its maximum (Fig. 2(a)). All the absorption spectra can be well fitted by the Lorentzian line shape with two components, corresponding to the exciton and trion resonances, respectively (e.g., refer to Fig. S2 in the ESM). The decreasing of the oscillator strength and the broadening of the A excitons are observed. In particular, a slight redshift of the exciton resonance appears for all pump fluences (Fig. 2(d)), suggesting that the carrier-screening induced decrease of E_g is slightly larger than the decreasing of E_B (inset of Fig. 2(d)). In addition, the redshift of A excitons in the first sub-ps regime is also observed in monolayer MoS_2 (Fig. S5 in the ESM), consistent with above-bandgap pump excitations in WS_2 (Fig. 2(a) and Fig. S4 in the ESM), which further confirms that such scenario is not influenced by the subtle difference of band structures in different 2D TMDs, in good agreement with recent theoretical calculations [52]. Further, the nonequilibrium hot carriers relax down towards the band edge through carrier–phonon and carrier–carrier interactions, and subsequently form excitons and/or trions [30, 53]. As shown in Fig. S7 in the ESM, by fitting the kinetics of the sub-ps PIA feature for the probe energy of ~ 2.01 eV at low pump fluence, the hot-carrier relaxation time is obtained to be ~ 0.33 ± 0.03 ps under the pump excitation of 3.35 eV. Since the carrier–carrier Coulomb interaction can be further amplified with the increase of pump fluence [53], it is expected that the hot-carrier relaxation time becomes shorter and consequently the exciton/trion population buildups faster. Indeed, explicit signatures from the contribution of excitons are observed in the first sub-ps time regime, including the appearing of multi-exponential decay for the sub-ps PIA feature (Fig. S7 in the ESM) and the decreased redshift of A excitons (Fig. 2(d)), at the pump fluence larger than ~ 10.0 μJ/cm^2. We will then focus on the exciton population dynamics at longer delay times.

Figure 3(a) shows pump-fluence dependent TA spectra at Δt = 1.0 ps for the excitation energy of 3.35 eV at 10 K. The TA spectra for A excitons have a dispersive profile with the PIA feature at higher energies (> ~ 2.10 eV) and a prominent PIB peak at energies slightly below E_A. The PIB/PIA peak for A excitons shifts to lower/higher energy with increasing pump fluence, i.e., the exciton density, respectively. This behavior strongly indicates that the blueshift of A excitons results from robust exciton–exciton interactions [45, 46]. In semiconductors, exciton population contributes to the nonlinear optical response in two major ways. One is the reduction of exciton oscillator strength due to the phase-space filling (Pauli blocking), and the other is the self-energy renormalization and broadening arising from exciton–exciton interactions [45, 54]. The prominent PIB signature of the A excitons and its pump-fluence dependence are mainly attributed to the phase-space filling, while the PIA feature is largely determined by the exciton–exciton interactions. Interestingly, the blueshift of the exciton energy observed at all pump fluence unambiguously reveals the nature of the repulsive Coulomb interaction between excitons in the 2D limit. Nevertheless, the exciton blueshift is rather small and estimated to be less than ~ 1.0 meV at a pump fluence of ~ 19 μJ/cm^2 (Fig. S8 in the ESM), which could be the reason that other optical spectroscopy techniques (like the time-resolved photoluminescence) with lower sensitivities cannot access such small changes [55].

Therefore, we can conclude that the decreased redshift of A excitons at Δt = 0.15 ps (Fig. 2(d)) is an overall response from the reduced carrier screening effect and enhanced exciton–exciton interactions with the increase of pump fluence. Furthermore, the blueshift of A excitons decays following the exciton recombination as show in Fig. 2(a), determined the second time regime with a timescale of few to several tens of ps depending on the pump fluences.

The exciton decay mechanism in monolayer TMDs is yet to be fully understood due to the complicated intrinsic and extrinsic factors, such as the influences of dark exciton states, defects, lattice temperature and pump fluence [31, 42, 43, 49, 56]. The decay kinetics extracted at E_A = 2.09 eV at two different pump fluences is shown in Fig. 3(b). The kinetics can be well fitted well by using a sum of biexponential components with decay times of τ_1 = 0.32 ± 0.05 ps and τ_2 = 1.16 ± 0.15 ps at the low pump fluence (1.9 μJ/cm^2). In addition to these two fast decays, a slow process with a decay time of τ_3 =23.99 ± 2.37 ps occurs and dominates at higher pump fluences (e.g., 12.0 and 24.0 μJ/cm^2) (Fig. S3(c) in the ESM). These results are drastically different with those measured at room temperature shown in Fig. S4 in the ESM. At room temperature, the decay of A excitons in monolayer WS_2 occurs at a timescale of ns at low pump fluence and becomes shorter at high pump fluence [48, 50]. Here, we attribute the τ_1 to the hot carrier relaxation process as discussed above, τ_2 to the intrinsic radiative lifetime of A excitons at low temperature and τ_3 to the nonradiative exciton–exciton annihilation process as schematically shown in Fig. 3(c), in which exciton–exciton scattering (EES) and exciton–exciton annihilation (EEA) processes are annotated. The A excitons at the band edge with momenta close to 0 ($K \approx 0$), namely within the light cone, can recombine radiatively. While for the exciton with large momenta (referred as momentum-forbidden dark excitons), they can either relax down to become bright excitons or recombine non-radiatively via direct phonon-emission to heat up the lattice, Auger processes and/or defects [30, 31, 50]. Ideally, the intrinsic radiative lifetime of A excitons is calculated to be on the order of several hundred fs because of the giant exciton oscillator strength in 2D TMDs at 0 K [57, 58]. However, at finite temperature, the radiative lifetime of excitons increases due to their thermalization through the exciton–phonon interactions [57, 58]. The observed exciton radiative lifetime τ_2 (~ 1.2 ps) for monolayer WS_2 at 10 K agrees very well with theoretical predictions [57, 58]. We believe that the defects play a minor role since no such fast exciton decay process is observed with low pump fluence at room temperature (Fig. S4 in the ESM).

With an increasing exciton density, the EES is substantially enhanced, which leads to a nonthermal distribution of excitons with a large fraction of momentum-forbidden dark excitons (Fig. 3(c)) [27, 49, 50, 59]. Although the momentum-forbidden dark excitons can relax down to emit photons, most of them decays primarily through the Auger-type EEA process owing to the strongly enhanced Coulomb interaction in 2D TMDs [27, 49, 50, 60, 61]. As a consequence, an effective radiative lifetime (τ_{eff}) of A excitons, which captures the interplay between bright and dark excitons with increasing pump fluence, is fully determined by the long decay time (τ_3, for instance) of the Auger recombination for the pump fluence in the saturation regime [48, 50]. On the other hand, at room temperature the ns decay time of A excitons at low excitation density arises from the more complicated interplays among the bright, momentum-forbidden dark excitons and particularly the long-lived spin-forbidden dark excitons which is only a few tens of meV below the bright excitons in monolayer TMDs [6, 56]. Similarly, the EEA becomes the main decay channel for excitons at high densities at room temperature [48, 50]. It is also noteworthy to mention that the efficient EEA process greatly suppresses the formation of biexcitons, and indeed there is no signature of biexcitons observed in the TA spectra for all pump fluences at both room and low temperatures in our studies.

Following the decay of exciton population, a redshift of A excitons is evidenced by the presence of a dispersive TA spectra centered at E_A shown in Figs. 2(a)–2(c) and 3(d) in the third time regime (Δt > ~ 10.0 ps). The exciton redshift reaches its maximum value at Δt ~ 30.0 ps, and then decays until ~ 200.0 ps slightly depending on the pump fluence. At room temperature, the redshift of A excitons is observed, which was ascribed to the atom-like attraction between excitons or lattice heating induced by the EEA process [42, 43]. However, the comprehensive results presented here suggest a different scenario. First of all, the exciton–exciton interaction leads to

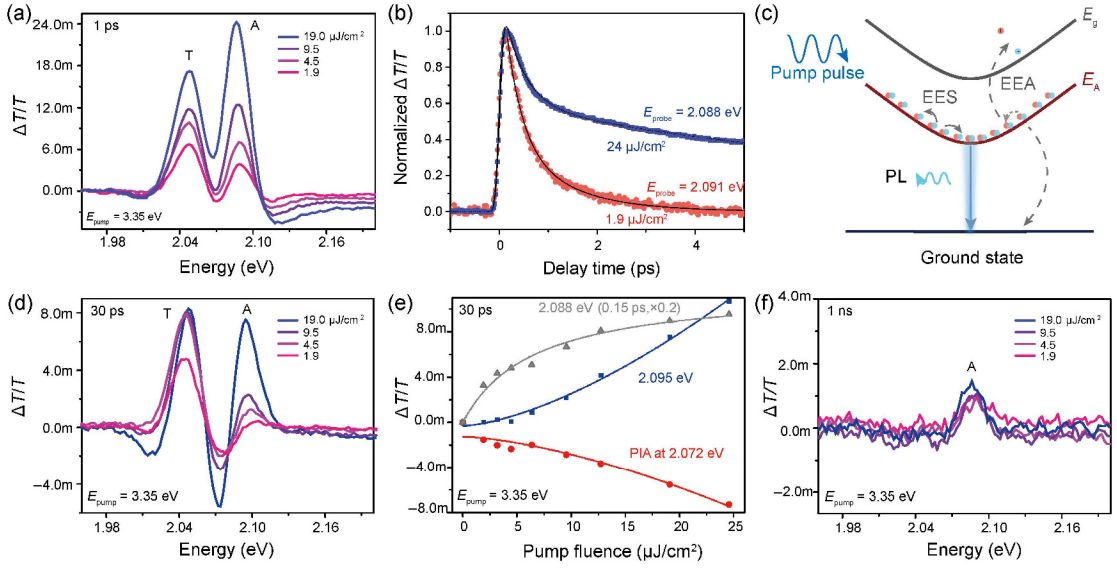

Figure 3 The blue- and red-shift of exciton energy arising from Coulombic exciton–exciton interaction and Auger photocarrier generation, respectively. (a) Pump-fluence dependent TA spectra for E_{pump} = 3.35 eV at Δt = 1 ps. (b) The normalized TA kinetics at E_{probe} = ~ 2.09 eV for the pump fluence of 1.9 μJ/cm^2 (red curve) and 24.0 μJ/cm^2 (blue curve), fitted with bi- and multi-exponential decay (black lines), respectively. (c) Schematic of band structure and exciton radiative decay (i.e., PL), EES and the Auger recombination process of EEA in monolayer WS_2. (d) Pump-fluence dependent TA spectra for E_{pump} = 3.35 eV at Δt = 30.0 ps. (e) The $\Delta T/T$ of the PIA and PIB for different probe energies as a function of the pump fluence at Δt = 30.0 ps, and the results for the PIB at Δt = 0.15 ps are shown as a comparison. The colored lines are the fitting results with the superlinear function and the gray line with a saturation function. (f) Pump-fluence dependent TA spectra for E_{pump} = 3.35 eV at Δt = 1.0 ns.

the blueshift of A excitons as discussed above. Secondly, as schematically shown in Fig. 3(c), in the EEA process one exciton recombines non-radiatively and transfers its energy to the second one which is promoted to the continuum band to become free carriers. The EEA-excited free carriers will subsequently relax down towards the band edge via carrier–phonon and carrier–carrier interactions. However, the phonon emitted during the carrier relaxation process at such low carrier densities could not give rising to notable changes of the lattice temperature [30, 42, 43]. Therefore, the redshift origin is the same as that observed in the first sub-ps time regime, i.e., the carrier screening effect.

Figure 3(e) shows the pump-fluence dependent $\Delta T/T$ of the PIB/PIA around E_A at Δt = 30.0 ps. The PIB results (triangle) at E_A for delay time 0.15 ps are shown for a comparison. At those two delay time scales, the exciton exhibits the most pronounced red shift (Fig. 2(a)). As shown in Fig. 3(e), the exciton redshift probed at 2.095 eV shows a super-linear growth with increasing pump fluence, in a stark contrast to that at 0.15 ps with a saturating behavior. This super-linear dependence indicates that charge carriers are mainly generated by the bimolecular EEA process. At high pump fluence, the bright A excitons primarily decay via EEA, creating a dynamical density ratio between EEA-excited free carriers and excitons as a function of delay time. Indicated by the temporal evolution of the A exciton redshift, the density ratio reaches its maximum at ~ 30.0 ps, and then decreases over several hundreds of ps (Fig. 2(a) and Fig. S3 in the ESM). At the subsequent longer delay times (up to the limitation of our measurements, ~ 8.0 ns), a quasi-equilibrium state is reached, showing a small population of bright A exciton (Fig. 3(f)). It is interesting that at low pump fluence the exciton redshift and similar dynamics are evident, although the bright excitons are mainly depleted in the ps timescale via radiative recombination. Inherently, the bright exciton is only a small portion of total exciton density even at low pump fluence, as the density of dark excitons can be up to several orders of magnitude higher than that of bright ones in monolayer TMDs at low temperature calculated theoretically [56]. The Auger-type EEA is also the dominant decay channel for the long-lived spin-forbidden dark excitons as predicted by recent theories [49, 56], thus contributing to the free carriers significantly. Therefore, the efficient EEA for bright and dark excitons puts the system in a nonequilibrium state at unexpected long delay times.

Lastly, we will discuss the dynamics of the negative trions at 10 K, which shows considerable difference from that of excitons. Firstly, as shown in Fig. 4(a), the PIB kinetics at the trion energy (E_T) shows an ultrafast decay component of ~ 0.6 ± 0.06 ps and a slow one of 108.7 ± 12.0 ps at low pump fluence. The ultrafast decay is related to the hot carrier relaxation and the formation of exciton and trion, while the slow decay component is primarily attributed to the radiative decay of trions. The longer lifetime is an intrinsic characteristic of the three-body quasiparticles, resulting from the reduced probability for the electron left behind when the trion recombines to find available phase space at the conduction band edge owing to the Pauli blocking [58]. With the increasing pump fluence, the population of trions saturates at an excitation density of ~ 10^{12} cm^{-2} is shown in the inset of Fig. 4(a), agreeing well with the estimated electron doping concentration discussed above. The different saturation density for exciton (Fig. 3(e)) and trions (Fig. 4(a)) also suggests no noticeable photo-doping effect occurred during the pump-probe experiments with the pump fluence below 24 μJ/cm^2 [60, 61]. Further, the decay time of trions becomes faster with the increase of pump fluence because of the trion–trion annihilation (Fig. S9 in the ESM). Secondly, the binding energy of trions increases with increasing pump fluence in the first sub-ps time regime presented in Figs. 2(c) and 4(b). This anomalous behavior is not caused by the carrier screening effects which would be expected to induce an opposite trend as discussed above [52]. Possible contributions from the trion fine structures are also not likely at such low electron doping concentration [33], while many-body correlations between excitons and trions may play an important role [32]. However, further experimental investigations on monolayer samples with tunable doping concentrations are needed to understand the many-body physics and fascinating valley-contrasting properties of excitonic complexes such as trions, biexcitons and charged biexcitons [23, 25, 26, 32].

3 Conclusions

In summary, we have studied the exciton and trion dynamics in monolayer TMDs by using ultrafast transient absorption spectroscopy. The exciton resonance shows a distinct red-blue-red shift at three different time regimes following above-bandgap optical excitations, resulting from many-body interactions among free carriers, bright and dark excitons. The many-body interactions and associated transient excitonic nonlinearities can be well-tuned through varying lattice temperature and excitation energy and density. An ultrafast radiative lifetime of A excitons in monolayer WS_2 is observed to be ~1.2 ps at 10 K. The robust exciton–exciton annihilation for both bright and dark excitons leads to a non-equilibrium state of the photoexcited system in the nanosecond timescale.

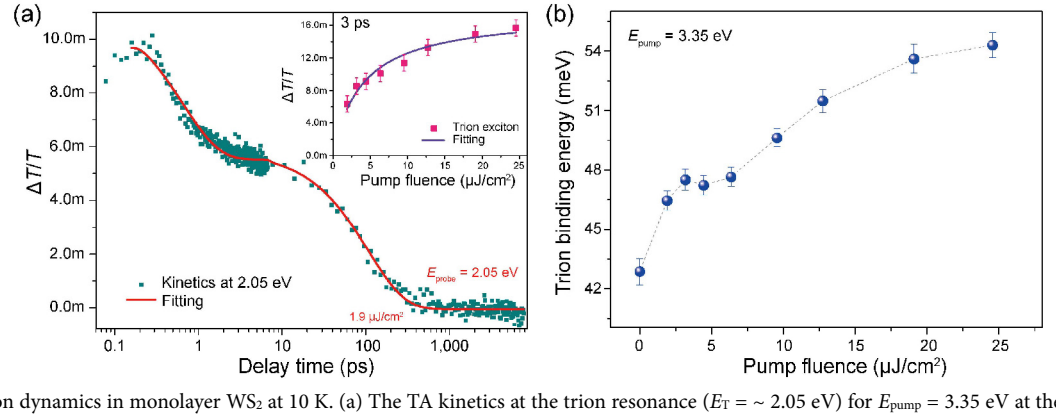

Figure 4 Trion dynamics in monolayer WS_2 at 10 K. (a) The TA kinetics at the trion resonance (E_T = ~ 2.05 eV) for E_{pump} = 3.35 eV at the pump fluence of 1.9 μJ/cm^2, fitted with bi-exponential decays (red solid lines). The inset shows the $\Delta T/T$ of the PIB at E_T as a function of pump fluence at Δt = 3.0 ps. (b) The evolution of trion binding energy (ΔE) as a function of pump fluence for E_{pump} = 3.35 eV at Δt = 1 ps.

Furthermore, the negative trions in monolayer WS_2 show an intrinsic radiative lifetime of ~ 108.7 ps at low temperature and an unusual energy renormalization at the sub-ps delay time upon the non-resonant excitations. Our results present a comprehensive physical picture of the distinct exciton dynamics and many-body interactions in 2D TMDs and will shed light on their potential applications in novel photonic and optoelectronic devices. On the other hand, the microscopic understanding of many-body physics in 2D semiconductors is still in its infancy, and a plethora of quantum phenomena are waiting for future investigations.

4 Materials and methods

4.1 Sample preparations

The monolayer TMDs were mechanically exfoliated from bulk crystals and transferred on sapphire substrates. The large-area and high-quality monolayer samples were characterized by optical contrast, absorption and photoluminescence spectroscopy, and atomic force microscopy (AFM).

4.2 Optical spectroscopy measurements

The steady-state absorption/transmission spectra at room temperature were measured by using a micro-spectrophotometer. The ultrafast pump-probe measurements were conducted by employing a commercial transient absorption spectrometer (Ultrafast Systems, USA). The 800 nm output pulse laser (1 kHz repetition rate, ~ 100 fs pulse width) from a Ti:sapphire regenerative amplifier (Spectra-Physics Spitfire) was split into two paths. One beam went through a mechanical delay stage to pump a sapphire crystal to generate a light continuum to serve as the probe pulse. The second beam was sent to an optical parametric amplifier (Spectra-Physics TOPAS) to generate pump pulses (260–2,000 nm). The pump and probe pulses with a cross-polarization configuration were collinearly focused on samples with a beam size of about 100 and 50 μm, respectively, by using parabolic mirrors. A mechanical chopper with a synchronized readout of a CMOS detector was used for acquisitions of probe spectra with and without pump-induced changes, enabling the measurement of a differential transmission. The spectra resolution was ~ 1.0 nm across the detecting range. For each transient absorption spectrum, three scans were performed to ensure the repeatability for the obtained results. The steady-state and ultrafast optical spectra at low temperature were conducted by using a liquid-helium cryostat.

Acknowledgments

Q. H. X. gratefully acknowledges the support from Singapore Ministry of Education via AcRF Tier 3 Programme (No. MOE2018-T3-1-002) and Tier 2 project (No. MOE2017-T2-1-040), and Singapore National Research Foundation via NRF-ANR project (No. NRF2017-NRF-ANR005 2D-Chiral).

Dedication

I would like to dedicate this article to Professor Charles Lieber (Charlie, as how group members and alumni call him). I was fortunate to work with him as a postdoctoral fellow for three years (2006–2009), since then we have had many interactions in the past ten years. Charlie is a great scientist and enthusiastic educator. In his eyes, science has no boundaries. Rather having the boundary between disciplines defines our research, we should have the courage to explore the directions that we do not know much previously. Over the interactions with him through emails or in-person discussions, he always showed us how we should critically think and identify the most important scientific questions to address. A great example is how unprecedentedly he advanced the early generation of nanowire-based nanoelectronics-biological sensors to the latest-generation of syringe-injectable flexible mesh electronics capable of probing human brain in real time. Charlie works hard to help students or postdoctoral fellows. Very often, we had chances to meet him in person a few times a week to discuss progress. When it came to critical moment of project, it was not rare at all that we could meet him a few times a day. Given the various commitments he had and his extremely busy schedule, it was like a miracle how he managed his time. What was behind that must be the sacrifice of his leisure and personal life. When it comes to reference letters for different career stages, we can always count on him to strongly support us. No matter how much I want to thank him, whatever I could do is not enough. Nonetheless, what I can do is to learn from Charlie, and bring it on to pass the spirit to younger generations of my own students and postdoctoral fellows.

Charlie, Happy 60th Year's Birthday! We look forward to celebrating your achievements again 10 years later!

Dedicated by the corresponding author Qihua Xiong.

References

[1] Mak, K. F.; Lee, C.; Hone, J.; Shan, J.; Heinz, T. F. Atomically thin MoS_2: A new direct-gap semiconductor. *Phys. Rev. Lett.* **2010**, *105*, 136805.

[2] Splendiani, A.; Sun, L.; Zhang, Y. B.; Li, T. S.; Kim, J.; Chim, C. Y.; Galli, G.; Wang, F. Emerging photoluminescence in monolayer MoS_2. *Nano Lett.* **2010**, *10*, 1271–1275.

[3] Wang, Q. H.; Kalantar-Zadeh, K.; Kis, A.; Coleman, J. N.; Strano, M. S. Electronics and optoelectronics of two-dimensional transition metal dichalcogenides. *Nat. Nanotechnol.* **2012**, *7*, 699–712.

[4] Chhowalla, M.; Shin, H. S.; Eda, G.; Li, L. J.; Loh, K. P.; Zhang, H. The chemistry of two-dimensional layered transition metal dichalcogenide nanosheets. *Nat. Chem.* **2013**, *5*, 263–275.

[5] Novoselov, K. S.; Mishchenko, A.; Carvalho, A.; Castro Neto, A. H. 2D Materials and van der Waals heterostructures. *Science* **2016**, *353*, aac9439.

[6] Mak, K. F.; Xiao, D.; Shan, J. Light–valley interactions in 2D semiconductors. *Nat. Photonics* **2018**, *12*, 451–460.

[7] Qiu, D. Y.; da Jornada, F. H.; Louie, S. G. Optical spectrum of MoS_2: Many-body effects and diversity of exciton states. *Phys. Rev. Lett.* **2013**, *111*, 216805.

[8] Wang, G.; Chernikov, A.; Glazov, M. M.; Heinz, T. F.; Marie, X.; Amand, T.; Urbaszek, B. *Colloquium*: Excitons in atomically thin transition metal dichalcogenides. *Rev. Mod. Phys.* **2018**, *90*, 021001.

[9] Yin, Z. Y.; Li, H.; Li, H.; Jiang, L.; Shi, Y. M.; Sun, Y. H.; Lu, G.; Zhang, Q.; Chen, X. D.; Zhang, H. Single-layer MoS_2 phototransistors. *ACS Nano* **2012**, *6*, 74–80.

[10] Lopez-Sanchez, O.; Lembke, D.; Kayci, M.; Radenovic, A.; Kis, A. Ultrasensitive photodetectors based on monolayer MoS_2. *Nat. Nanotechnol.* **2013**, *8*, 497–501.

[11] Withers, F.; Del Pozo-Zamudio, O.; Mishchenko, A.; Rooney, A. P.; Gholinia, A.; Watanabe, K.; Taniguchi, T.; Haigh, S. J.; Geim, A. K.; Tartakovskii, A. I. et al. Light-emitting diodes by band-structure engineering in van der Waals heterostructures. *Nat. Mater.* **2015**, *14*, 301–306.

[12] Wang, S. F.; Wang, J. Y.; Zhao, W. J.; Giustiniano, F.; Chu, L. Q.; Verzhbitskiy, I.; Zhou Yong, J.; Eda, G. Efficient carrier-to-exciton conversion in field emission tunnel diodes based on MIS-type van der Waals heterostack. *Nano Lett.* **2017**, *17*, 5156–5162.

[13] Lee, J.; Mak, K. F.; Shan, J. Electrical control of the valley Hall effect in bilayer MoS_2 transistors. *Nat. Nanotechnol.* **2016**, *11*, 421–425.

[14] Schaibley, J. R.; Yu, H. Y.; Clark, G.; Rivera, P.; Ross, J. S.; Seyler, K. L.; Yao, W.; Xu, X. D. Valleytronics in 2D materials. *Nat. Rev. Mater.* **2016**, *1*, 16055.

[15] Rivera, P.; Yu, H. Y.; Seyler, K. L.; Wilson, N. P.; Yao, W.; Xu, X. D. Interlayer valley excitons in heterobilayers of transition metal dichalcogenides. *Nat. Nanotechnol*. **2018**, *13*, 1004–1015.

[16] Unuchek, D.; Ciarrocchi, A.; Avsar, A.; Watanabe, K.; Taniguchi, T.; Kis, A. Room-temperature electrical control of exciton flux in a van der Waals heterostructure. *Nature* **2018**, *560*, 340–344.

[17] Wu, S. F.; Buckley, S.; Schaibley, J. R.; Feng, L. F.; Yan, J. Q.; Mandrus, D. G.; Hatami, F.; Yao, W.; Vuckovic, J.; Majumdar, A. et al. Monolayer semiconductor nanocavity lasers with ultralow thresholds. *Nature* **2015**, *520*, 69–72.

[18] Ye, Y.; Wong, Z. J.; Lu, X. F.; Ni, X. J.; Zhu, H. Y.; Chen, X. H.; Wang, Y.; Zhang, X. Monolayer excitonic laser. *Nat. Photonics* **2015**, *9*, 733–737.

[19] Chernikov, A.; Berkelbach, T. C.; Hill, H. M.; Rigosi, A.; Li, Y. L.; Aslan, O. B.; Reichman, D. R.; Hybertsen, M. S.; Heinz, T. F. Exciton binding energy and nonhydrogenic Rydberg series in monolayer WS_2. *Phys. Rev. Lett*. **2014**, *113*, 076802.

[20] Chernikov, A.; Ruppert, C.; Hill, H. M.; Rigosi, A. F.; Heinz, T. F. Population inversion and giant bandgap renormalization in atomically thin WS_2 layers. *Nat. Photonics* **2015**, *9*, 466–470.

[21] Liu, B.; Zhao, W. J.; Ding, Z. J.; Verzhbitskiy, I.; Li, L. J.; Lu, J. P.; Chen, J. Y.; Eda, G.; Loh, K. P. Engineering bandgaps of monolayer MoS_2 and WS_2 on fluoropolymer substrates by electrostatically tuned many-body effects. *Adv. Mater*. **2016**, *28*, 6457–6464.

[22] Mak, K. F.; He, K. L.; Lee, C.; Lee, G. H.; Hone, J.; Heinz, T. F.; Shan, J. Tightly bound trions in monolayer MoS_2. *Nat. Mater*. **2013**, *12*, 207–211.

[23] Barbone, M.; Montblanch, A. R. P.; Kara, D. M.; Palacios-Berraquero, C.; Cadore, A. R.; De Fazio, D.; Pingault, B.; Mostaani, E.; Li, H.; Chen, B. et al. Charge-tuneable biexciton complexes in monolayer WSe_2. *Nat. Commun*. **2018**, *9*, 3721.

[24] You, Y. M.; Zhang, X. X.; Berkelbach, T. C.; Hybertsen, M. S.; Reichman, D. R.; Heinz, T. F. Observation of biexcitons in monolayer WSe_2. *Nat. Phys*. **2015**, *11*, 477–481.

[25] Li, Z. P.; Wang, T. M.; Lu, Z. G.; Jin, C. H.; Chen, Y. W.; Meng, Y. Z.; Lian, Z.; Taniguchi, T.; Watanabe, K.; Zhang, S. B. et al. Revealing the biexciton and trion-exciton complexes in BN encapsulated WSe_2. *Nat. Commun*. **2018**, *9*, 3719.

[26] Steinhoff, A.; Florian, M.; Singh, A.; Tran, K.; Kolarczik, M.; Helmrich, S.; Achtstein, A. W.; Woggon, U.; Owschimikow, N.; Jahnke, F. et al. Biexciton fine structure in monolayer transition metal dichalcogenides. *Nat. Phys*. **2018**, *14*, 1199–1204.

[27] Poellmann, C.; Steinleitner, P.; Leierseder, U.; Nagler, P.; Plechinger, G.; Porer, M.; Bratschitsch, R.; Schüller, C.; Korn, T.; Huber, R. Resonant internal quantum transitions and femtosecond radiative decay of excitons in monolayer WSe_2. *Nat. Mater*. **2015**, *14*, 889–893.

[28] Shi, H. Y.; Yan, R. S.; Bertolazzi, S.; Brivio, J.; Gao, B.; Kis, A.; Jena, D.; Xing, H. G.; Huang, L. B. Exciton dynamics in suspended monolayer and few-layer MoS_2 2D crystals. *ACS Nano* **2013**, *7*, 1072–1080.

[29] Ceballos, F.; Cui, Q. N.; Bellus, M. Z.; Zhao, H. Exciton formation in monolayer transition metal dichalcogenides. *Nanoscale* **2016**, *8*, 11681–11688.

[30] Steinleitner, P.; Merkl, P.; Nagler, P.; Mornhinweg, J.; Schüller, C.; Korn, T.; Chernikov, A.; Huber, R. Direct observation of ultrafast exciton formation in a monolayer of WSe_2. *Nano Lett*. **2017**, *17*, 1455–1460.

[31] Wang, H. N.; Zhang, C. J.; Rana, F. Ultrafast dynamics of defect-assisted electron–hole recombination in monolayer MoS_2. *Nano Lett*. **2015**, *15*, 339–345.

[32] Hao, K.; Specht, J. F.; Nagler, P.; Xu, L. X.; Tran, K.; Singh, A.; Dass, C. K.; Schüller, C.; Korn, T.; Richter, M. et al. Neutral and charged inter-valley biexcitons in monolayer $MoSe_2$. *Nat. Commun*. **2017**, *8*, 15552.

[33] Plechinger, G.; Nagler, P.; Arora, A.; Schmidt, R.; Chernikov, A.; del Águila, A. G.; Christianen, P. C. M.; Bratschitsch, R.; Schuller, C.; Korn, T. Trion fine structure and coupled spin-valley dynamics in monolayer tungsten disulfide. *Nat. Commun*. **2016**, *7*, 12715.

[34] Guo, L.; Wu, M.; Cao, T.; Monahan, D. M.; Lee, Y. H.; Louie, S. G.; Fleming, G. R. Exchange-driven intravalley mixing of excitons in monolayer transition metal dichalcogenides. *Nat. Phys*. **2019**, *15*, 228–232.

[35] Schmidt, R.; Berghäuser, G.; Schneider, R.; Selig, M.; Tonndorf, P.; Malić, E.; Knorr, A.; Michaelis de Vasconcellos, S.; Bratschitsch, R. Ultrafast Coulomb-induced intervalley coupling in atomically thin WS_2. *Nano Lett*. **2016**, *16*, 2945–2950.

[36] Hao, K.; Moody, G.; Wu, F. C.; Dass, C. K.; Xu, L. X.; Chen, C. H.; Sun, L. Y.; Li, M. Y.; Li, L. J.; MacDonald, A. H. et al. Direct measurement of exciton valley coherence in monolayer WSe_2. *Nat. Phys*. **2016**, *12*, 677–682.

[37] Bertoni, R.; Nicholson, C. W.; Waldecker, L.; Hübener, H.; Monney, C.; De Giovannini, U.; Puppin, M.; Hoesch, M.; Springate, E.; Chapman, R. T. et al. Generation and evolution of spin-, valley-, and layer-polarized excited carriers in inversion-symmetric WSe_2. *Phys. Rev. Lett*. **2016**, *117*, 277201.

[38] Yan, T. F.; Yang, S. Y.; Li, D.; Cui, X. D. Long valley relaxation time of free carriers in monolayer WSe_2. *Phys. Rev. B* **2017**, *95*, 241406.

[39] Mai, C.; Barrette, A.; Yu, Y. F.; Semenov, Y. G.; Kim, K. W.; Cao, L. Y.; Gundogdu, K. Many-body effects in valleytronics: Direct measurement of valley lifetimes in single-layer MoS_2. *Nano Lett*. **2014**, *14*, 202–206.

[40] Cunningham, P. D.; Hanbicki, A. T.; McCreary, K. M.; Jonker, B. T. Photoinduced bandgap renormalization and exciton binding energy reduction in WS_2. *ACS Nano* **2017**, *11*, 12601–12608.

[41] Hong, X. P.; Kim, J.; Shi, S. F.; Zhang, Y.; Jin, C. H.; Sun, Y. H.; Tongay, S.; Wu, J. Q.; Zhang, Y. F.; Wang, F. Ultrafast charge transfer in atomically thin MoS_2/WS_2 heterostructures. *Nat. Nanotechnol*. **2014**, *9*, 682–686.

[42] Ruppert, C.; Chernikov, A.; Hill, H. M.; Rigosi, A. F.; Heinz, T. F. The role of electronic and phononic excitation in the optical response of monolayer WS_2 after ultrafast excitation. *Nano Lett*. **2017**, *17*, 644–651.

[43] Sie, E. J.; Steinhoff, A.; Gies, C.; Luo, C. H.; Ma, Q.; Rosner, M.; Schönhoff, G.; Jahnke, F.; Wehling, T. O.; Lee, Y. H. et al. Observation of exciton redshift-blueshift crossover in monolayer WS_2. *Nano Lett*. **2017**, *17*, 4210–4216.

[44] Yuan, L.; Chung, T. F.; Kuc, A.; Wan, Y.; Xu, Y.; Chen, Y. P.; Heine, T.; Huang, L. B. Photocarrier generation from interlayer charge-transfer transitions in WS_2-graphene heterostructures. *Sci. Adv*. **2018**, *4*, e1700324.

[45] Wake, D. R.; Yoon, H. W.; Wolfe, J. P.; Morkoç, H. Response of excitonic absorption spectra to photoexcited carriers in GaAs quantum wells. *Phys. Rev. B* **1992**, *46*, 13452–13460.

[46] Manzke, G.; Henneberger, K.; May, V. Many-exciton theory for multiple quantum-well structures. *Phys. Status Solidi B* **1987**, *139*, 233–239.

[47] Aivazian, G.; Yu, H. Y.; Wu, S. F.; Yan, J. Q.; Mandrus, D. G.; Cobden, D.; Yao, W.; Xu, X. D. Many-body effects in nonlinear optical responses of 2D layered semiconductors. *2D Mater*. **2017**, *4*, 025024.

[48] Cunningham, P. D.; McCreary, K. M.; Jonker, B. T. Auger recombination in chemical vapor deposition-grown monolayer WS_2. *J. Phys. Chem. Lett*. **2016**, *7*, 5242–5246.

[49] Danovich, M.; Zólyomi, V.; Fal'ko, V. I.; Aleiner, I. L. Auger recombination of dark excitons in WS_2 and WSe_2 monolayers. *2D Mater*. **2016**, *3*, 035011.

[50] Sun, D. Z.; Rao, Y.; Reider, G. A.; Chen, G. G.; You, Y. M.; Brézin, L.; Harutyunyan, A. R.; Heinz, T. F. Observation of rapid exciton-exciton annihilation in monolayer molybdenum disulfide. *Nano Lett*. **2014**, *14*, 5625–5629.

[51] Mouri, S.; Miyauchi, Y.; Toh, M.; Zhao, W. J.; Eda, G.; Matsuda, K. Nonlinear photoluminescence in atomically thin layered WSe_2 arising from diffusion-assisted exciton-exciton annihilation. *Phys. Rev. B* **2014**, *90*, 155449.

[52] Steinhoff, A.; Rösner, M.; Jahnke, F.; Wehling, T. O.; Gies, C. Influence of excited carriers on the optical and electronic properties of MoS_2. *Nano Lett*. **2014**, *14*, 3743–3748.

[53] Steinhoff, A.; Florian, M.; Rösner, M.; Lorke, M.; Wehling, T. O.; Gies, C.; Jahnke, F. Nonequilibrium carrier dynamics in transition metal dichalcogenide semiconductors. *2D Mater*. **2016**, *3*, 031006.

[54] Schmitt-Rink, S.; Chemla, D. S.; Miller, D. A. B. Theory of transient excitonic optical nonlinearities in semiconductor quantum-well structures. *Phys. Rev. B* **1985**, *32*, 6601–6609.

[55] Robert, C.; Lagarde, D.; Cadiz, F.; Wang, G.; Lassagne, B.; Amand, T.; Balocchi, A.; Renucci, P.; Tongay, S.; Urbaszek, B. et al. Exciton radiative lifetime in transition metal dichalcogenide monolayers. *Phys*. *Rev*. *B* **2016**, *93*, 205423.
[56] Steinhoff, A.; Florian, M.; Rösner, M.; Schönhoff, G.; Wehling, T. O.; Jahnke, F. Exciton fission in monolayer transition metal dichalcogenide semiconductors. *Nat*. *Commun*. **2017**, *8*, 1166.
[57] Palummo, M.; Bernardi, M.; Grossman, J. C. Exciton radiative lifetimes in two-dimensional transition metal dichalcogenides. *Nano Lett*. **2015**, *15*, 2794–2800.
[58] Wang, H. N.; Zhang, C. J.; Chan, W. M.; Manolatou, C.; Tiwari, S.; Rana, F. Radiative lifetimes of excitons and trions in monolayers of the metal dichalcogenide MoS_2. *Phys*. *Rev*. *B* **2016**, *93*, 045407.
[59] Nguyen, D. T.; Voisin, C.; Roussignol, P.; Roquelet, C.; Lauret, J. S.; Cassabois, G. Elastic exciton-exciton scattering in photoexcited carbon nanotubes. *Phys*. *Rev*. *Lett*. **2011**, *107*, 127401.
[60] Yuma, B.; Berciaud, S.; Besbas, J.; Shaver, J.; Santos, S.; Ghosh, S.; Weisman, R. B.; Cognet, L.; Gallart, M.; Ziegler, M. et al. Biexciton, single carrier, and trion generation dynamics in single-walled carbon nanotubes. *Phys*. *Rev*. *B* **2013**, *87*, 205412.
[61] Santos, S. M.; Yuma, B.; Berciaud, S.; Shaver, J.; Gallart, M.; Gilliot, P.; Cognet, L.; Lounis, B. All-optical trion generation in single-walled carbon nanotubes. *Phys*. *Rev*. *Lett*. **2011**, *107*, 187401.